Global Stability and Sensitivity Analysis of a Delayed Nutrient-Plankton Model Under Climate Change and Oceans Deoxygenation

Usman Solomon Alani[1*], Ibrahim Isa Adamu[2], Alhaji Tahir [3], Shamtang Benshak Musa[4]

[1, 2, 3]Department of Mathematics, Modibbo Adama University Yola, Adamawa state, Nigeria.

[4] Department of Statistics, Federal Polytechnic Kaltungo, Gombe state, Nigeria.

DOI: https://doi.org/10.51244/IJRSI.2026.1307000004

Received: 05 July 2026; Accepted: 10 July 2026; Published: 21 July 2026

ABSTRACT

Ocean deoxygenation driven by climate change and nutrient enrichment threatens marine ecosystems. This study analyzes a six-compartment nutrient-plankton-oxygen model incorporating three time-delays. Global asymptotic stability of the coexistence equilibrium is proved using the Lyapunov–Krasovskii method, indicating intrinsic ecosystem resilience. A novel threshold metric, the concentration number $C^* = 16$ is derived via next-generation matrix techniques, signaling significant bloom-induced deoxygenation risk. Sensitivity analysis identifies nutrient-to-phytoplankton conversion (k_1), nutrient uptake by phytoplankton (α), and external nutrient input (N_0) as strong positive drivers (+1.0 indices), while washout ($D = -0.8$) and phytoplankton mortality ($d_1 = -0.2$) exert mitigating effects. Results show that plankton-mediated oxygen production and greenhouse gas removal provide stabilizing feedback sufficient to offset warming-induced oxygen losses under the parameter values considered. These findings highlight nutrient management and plankton conservation as critical strategies to mitigate climate-driven ocean deoxygenation and preserve marine ecosystem sustainability.

Keywords: Climate change, Deoxygenation, Hypoxic, Ocean, Plankton.

INTRODUCTION

Marine Ecosystem

Marine ecosystems are maintained through complex interactions among nutrients, phytoplankton, zooplankton, and other aquatic organisms. Plankton are microscopic organisms that drift within water bodies and form the foundation of aquatic food webs (Pachiappan *et al.*, 2018). They are broadly classified into phytoplankton and zooplankton. Phytoplankton function as primary producers by converting solar energy into organic matter through photosynthesis, while zooplankton act as primary consumers that feed on phytoplankton and transfer energy to higher trophic levels (Rehim *et al.*, 2016; Sterpu *et al.*, 2023). These interactions regulate nutrient cycling, biological productivity, and ecosystem stability. Furthermore, phytoplankton communities are widely recognized as biological indicators of water quality and environmental change (Octavina *et al.,* 2025). Consequently, disturbances in plankton dynamics can alter food-web structures, reduce biodiversity, and affect the overall functioning and resilience of marine ecosystems.

Oxygen Production

The oceans play a crucial role in sustaining life on Earth by producing approximately 50–70% of the atmospheric oxygen through the photosynthetic activities of marine plankton, particularly phytoplankton and cyanobacteria (Laffoley *et al*., 2019; NOAA, 2024). Among these organisms, *Prochlorococcus*, one of the most abundant photosynthetic microorganisms in the ocean, contributes significantly to global oxygen production. In addition to generating oxygen, phytoplankton absorb substantial amounts of carbon dioxide, thereby contributing to the regulation of the global carbon cycle and climate system. Dissolved oxygen is essential for the survival, growth, and reproduction of marine organisms and serves as a key indicator of ocean health. However, global ocean

ISSN No. 2321-2705 | DOI: 10.51244/IJRSI |Volume XIII Issue VI June 2026

oxygen inventories have declined by approximately 2% since the 1960s, and further reductions are projected by the end of the century due to ocean warming, increased stratification, and reduced ocean ventilation (Schmidtko *et al*., 2017). Persistent oxygen depletion can result in hypoxia and the formation of dead zones, posing serious threats to marine biodiversity, fisheries, and ecosystem functioning.

Environmental Pollution

Environmental pollution and climate change have become major drivers of ocean degradation and deoxygenation. Since the Industrial Revolution, greenhouse gas concentrations have increased substantially due to fossil fuel combustion, deforestation, industrialization, and other human activities (Prentice *et al*., 2001; Gruber *et al*., 2019). As a result, atmospheric carbon dioxide levels have risen dramatically, intensifying the greenhouse effect and contributing to global warming. The oceans absorb nearly 90% of the excess heat trapped within the climate system, leading to increased ocean temperatures, altered circulation patterns, and reduced oxygen solubility (Rhein *et al*., 2013; Cheng *et al*., 2024). These changes accelerate the loss of dissolved oxygen and increase the vulnerability of marine ecosystems.

In addition to climate-related stressors, nutrient pollution from agricultural runoff, wastewater discharge, urban development, and industrial activities introduces excessive quantities of nitrogen and phosphorus into aquatic environments (Carpenter *et al*., 1998; Devlin and Brodie, 2023). Elevated nutrient concentrations stimulate excessive phytoplankton growth, often resulting in harmful algal blooms. Following bloom collapse, microbial decomposition of organic matter consumes large amounts of dissolved oxygen, creating hypoxic or anoxic conditions. This process, known as eutrophication, has been identified as one of the primary causes of oxygen depletion in coastal and estuarine ecosystems. The combined effects of greenhouse gas accumulation, ocean warming, and nutrient enrichment have intensified ocean deoxygenation, making it one of the most significant environmental challenges facing marine ecosystems in the twenty-first century. Despite considerable research efforts, the interactions among climate change, nutrient dynamics, biological processes, and oxygen depletion remain complex and require further investigation to support effective management and conservation strategies. Field observations conducted at three locations within the Lagos–Epe Lagoon system—Ikosi, Imope, and Egbin, revealed significant phytoplankton bloom events, with the highest bloom intensity recorded at Ikosi (approximately 6.5°N, 3.9°E) (Akagha *et al*., 2020). Dissolved oxygen concentrations declined to hypoxic levels ($DO \leq 2.6$ mg/L) across all three sites in January 2013, while oxygen levels at Ikosi remained below the recommended threshold ($DO \leq 5$ mg/L) in January 2014. These low oxygen conditions were attributed to excessive algal growth and the subsequent microbial decomposition of organic matter, which increased oxygen consumption within the lagoon ecosystem.

Mathematical Models

Mukherjee *et al.* (2019) proposed a mathematical model to detect Turing patterns in a three-species food chain model via amplitude equations. In developing their model, they assumed that the prey population grows logistically, while the intermediate predator and top predator both exhibit Holling type-II functional responses in grazing, with diffusion terms included for all three species under zero-flux boundary conditions. They further assumed that small random perturbations around the homogeneous steady state serve as initial conditions, and that the temporal model is locally asymptotically stable to allow for Turing instability. They adopted a compartment modeling approach to formulate a system of three reaction-diffusion equations: prey density $u_1(x,y,t)$, intermediate predator density $u_2(x,y,t)$, and top predator density $u_3(x,y,t)$. The analytical results of their study established conditions for Turing instability and derived amplitude equations via weakly nonlinear analysis, identifying thresholds for pattern emergence—spots, stripes, labyrinthine, and mixed states—near the Turing bifurcation boundary. Numerical simulations revealed that for fixed parameters and gradually increasing the top predator conversion efficiency a_4, the prey population exhibits a transition from hot spots to a mixture of hot spots and stripes, then to labyrinthine, followed by a mixture of cold spots and stripes, and finally to cold spots, while the intermediate and top predators show the opposite pattern (cold spots correspond to hot spots of prey, and vice versa). The results of their study further demonstrated that for lower diffusion coefficients (e.g., $d_3 = 0.4$), the pattern sequence shortens, and for very low diffusion ($d_3 = 0.1$), only cold spots (prey) and hot spots

ISSN No. 2321-2705 | DOI: 10.51244/IJRSI |Volume XIII Issue VI June 2026

(predators) appear throughout the Turing domain. Consequently, the authors concluded that the amplitude equation method is effective for predicting Turing patterns in three-species food chain models near the bifurcation threshold, and that the observed pattern transitions provide insight into spatial heterogeneity in multi-trophic ecosystems.

Zhuang *et al.* (2019) proposed a mathematical model to investigate the stability and Hopf bifurcation dynamics of a planktonic ecosystem comprising nontoxic phytoplankton, toxin-producing phytoplankton, and zooplankton under the combined effects of spatial diffusion and time delay. In developing their model, they assumed that the two phytoplankton populations share the same environmental resources and exhibit logistic growth, while zooplankton feed on both phytoplankton species. They further assumed that toxin-producing phytoplankton release harmful substances that reduce zooplankton growth and survival, that plankton species disperse spatially through Fickian diffusion, and that a time delay exists between the ingestion of toxic phytoplankton and the manifestation of its toxic effects on zooplankton. The authors also assumed a closed aquatic environment with homogeneous Neumann boundary conditions, implying that no species enters or leaves the habitat through its boundaries. They adopted a compartment modeling approach to formulate a system of three reaction–diffusion delay differential equations consisting of nontoxic phytoplankton density P(t), toxin-producing phytoplankton density T(t), and zooplankton density Z(t). The analytical results of their study established conditions for permanence, non-persistence, existence of positive equilibrium solutions, and local stability of the coexistence equilibrium. Furthermore, they derived criteria for delay-induced Hopf bifurcation and determined the direction and stability of bifurcating periodic solutions using center manifold and normal form theories. Numerical simulations revealed that when τ is below a critical value τ_0 ($\tau = 0.65$), the equilibrium remains asymptotically stable, but exceeding this threshold ($\tau = 25$) induces spatially homogeneous periodic solutions, with nontoxic phytoplankton exhibiting the largest oscillation amplitude. The results of their study further demonstrated that under different parameter sets, increasing τ can also lead to spatially inhomogeneous periodic solutions (at $\tau = 5.42$ on a larger domain). Thus, the authors concluded that toxin-induced time delay plays a crucial role in triggering periodic plankton blooms, and that controlling the delay or adding feedback mechanisms could help stabilize the aquatic ecosystem.

Misra *et al.* (2020) proposed a mathematical model to investigate the effects of budget allocation and time delay on the control of algal blooms in lake ecosystems. In developing their model, they assumed that nutrients enter the lake from external sources at a constant rate and are utilized by algae for growth, while a portion of dead algal biomass is converted back into nutrients through bacterial decomposition. They further assumed that government budget allocation for algal bloom control follows logistic growth and increases proportionally with the density of algae in the lake. The authors also assumed that a fraction of the allocated budget is used to restrict nutrient inflow into the lake, while the remaining portion is utilized for the direct removal of algae. In addition, they assumed that the effectiveness of budget allocation on nutrient reduction and algal removal is subject to saturation effects and that there exists a discrete time delay between the increase in algal density and the corresponding increase in budget allocation. They adopted a compartment modeling approach to formulate a system of three differential equations consisting of nutrient concentration N(t), algal density A(t), and budget allocation M(t), which was subsequently extended into a delay differential equation model by incorporating the delayed response of budget allocation. The analytical results of their study established the positivity, boundedness, permanence, and local stability properties of the system and identified four equilibrium states, namely the nutrient-only equilibrium, nutrient–budget equilibrium, nutrient–algae equilibrium, and coexistence equilibrium. Furthermore, they derived conditions for transcritical and Hopf bifurcations and proved that time delay can destabilize the coexistence equilibrium. Numerical simulations revealed that increasing the efficacy of budget for nutrient inflow control or algal removal can completely eradicate algae, while in the absence of external nutrient input the system exhibits bi-stability between an algae-free and a coexistence equilibrium. The results of their study further demonstrated that introducing time delay causes Hopf bifurcations, leading to limit cycles and eventually chaotic oscillations (confirmed by Poincaré maps and positive maximum Lyapunov exponents) as the delay increases (from $\tau = 20$ days cycles to $\tau = 190$ days chaos). Hence, the authors concluded that effective budget allocation—especially improving the efficacy of nutrient inflow control—is crucial for mitigating algal blooms, and that time delays in budget response can destabilize the system, requiring rapid action to prevent chaotic population swings.

ISSN No. 2321-2705 | DOI: 10.51244/IJRSI |Volume XIII Issue VI June 2026

Sekerci and Ozarslan (2020) proposed a mathematical model to investigate the respiration effect on oxygen–plankton dynamics using non-singular fractional-order derivatives. In developing their model, they assumed that phytoplankton are the primary producers of oxygen through photosynthesis, while zooplankton act as predators that feed on phytoplankton and consume oxygen through respiration. They further assumed that oxygen is naturally depleted in the aquatic environment, that phytoplankton growth depends on oxygen availability and is regulated by intraspecific competition, and that zooplankton grazing follows a Holling type II functional response. The authors also assumed a well-mixed, non-spatial aquatic ecosystem with no spatial gradients in oxygen concentration or plankton densities. They adopted a compartment modeling approach to formulate a system of three nonlinear differential equations consisting of oxygen concentration f(t), phytoplankton density g(t), and zooplankton density s(t), which was subsequently extended into fractional-order forms using the Caputo–Fabrizio and Atangana–Baleanu derivatives. The analytical results of their study established the existence of three equilibrium states, namely the extinction equilibrium, the zooplankton-free equilibrium, and the coexistence equilibrium, and derived local stability conditions through eigenvalue analysis. Numerical simulations using finite difference schemes revealed that as the fractional order α approaches 1, the solutions approximate the classical integer-order dynamics. The results of their study further demonstrated that for parameter values T=1.02 and $f_1 = 0.7$ with α=0.98, the system exhibits periodic oscillations; for T=0.92 and $f_1 = 0.7$, damping oscillations converge to a steady state; and for T=0.4 and $f_1 = 0.3$, oscillations decrease in size. Additionally, different initial conditions can lead to either limit cycle attractors or extinction. Consequently, the authors concluded that fractional derivatives with non-singular kernels (Caputo-Fabrizio and Atangana-Baleanu) provide more accurate and flexible modeling of oxygen-plankton dynamics compared to classical derivatives, and that the choice of fractional order and parameter values significantly influences system stability, oscillation behavior, and the onset of bifurcations.

Hong Yang (2022) proposed a mathematical model to investigate the global dynamics of a diffusive phytoplankton–zooplankton system in the presence of toxic-substance effects and time delay. In developing the model, the author assumed that toxin-producing phytoplankton grow logistically in the absence of predation, while zooplankton feed on phytoplankton according to a Holling type II functional response. He further assumed that the toxic effect of phytoplankton on zooplankton is not instantaneous but occurs after a discrete time delay representing the period between toxin ingestion and its harmful impact.

In addition, phytoplankton and zooplankton were assumed to disperse spatially through diffusion due to ocean currents, tides, and turbulence, while no species enters or leaves the habitat through its boundaries, resulting in homogeneous Neumann boundary conditions. The author adopted a compartment modeling approach to formulate a system of two reaction–diffusion delay differential equations consisting of toxin-producing phytoplankton density u(x,t) and zooplankton density v(x,t). The analytical results of their study established the uniform boundedness and positivity of solutions, proved that when τ=0τ=0 the positive equilibrium is globally attractive using upper-lower solution methods, and derived the characteristic equation to show that time delay induces Hopf bifurcation. Numerical simulations revealed that for parameters satisfying $2D_0 - T^2{}_0 > 0$ and $T^4{}_0 - 4T^2{}_0 D_0 + 4\theta^2\delta^2(1-\delta)^2 > 0$, the system is stable for $\tau = 7$ (below the critical value $\bar{\tau} \approx 12.15$) but undergoes Hopf bifurcation and produces periodic oscillations for $\tau = 22 > \bar{\tau}$. The results of their study further demonstrated, via global Hopf bifurcation theory, that for each $\tau > \tau^+_{n_0,k}$ the system has at least k+1 periodic solutions, and the direction and stability of bifurcating periodic solutions were determined by computing normal form coefficients. Thus, the author concluded that time delay is a key factor destabilizing the plankton system, causing periodic fluctuations in population densities, and that the diffusive delay model better reflects real-world plankton dynamics.

While substantial progress has been made in modelling nutrient–plankton ecosystems and climate-induced environmental changes, studies that examine the global stability and the sensitivity analysis of the jointly time-delayed nutrient–plankton interactions, ocean deoxygenation, and greenhouse gas effects within the marine ecosystems are still absent.

ISSN No. 2321-2705 | DOI: 10.51244/IJRSI |Volume XIII Issue VI June 2026

With this motivation, we set out to carry out the global stability analysis and the sensitivity analysis of a mathematical model on nutrient-plankton system with delay under climate change and ocean deoxygenation.

GLOBAL STABILITY ANALYSIS OF THE COEXISTENCE EQUILIBRIUM POINT:

We use the Lyapunov Krasovskii's Generalized Method for Global Stability to carry out the Global stability analysis of the coexistence equilibrium point:

The mathematical model employed in this analysis was adopted from Solomon *et al.* (2026);

$$\begin{cases} \frac{dN}{dt} = D(N_0 - N) - \alpha NP + m_1 d_1 P(t-\tau_1) + m_2 d_2 Z(t-\tau_2) - \sigma NT \\ \frac{dZ}{dt} = \frac{k_2 \beta PZ}{a+P} - \frac{k_3 \beta ZP(t-\tau_3)}{a+P(t-\tau_3)} - (D+d_2)Z - \varepsilon TZ - \phi GZ \\ \frac{dO}{dt} = \psi P - \mu TO - \delta wO - \pi_1 PO - \pi_2 ZO - \pi_3 GO \\ \frac{dP}{dt} = k_1 \alpha NP - (D+d_1)P - \frac{\beta PZ}{a+P} - vP^2 - hTP + \pi_1 PO \\ \frac{dT}{dt} = \theta_1 GT + \sigma NT - xT + \varepsilon TZ \\ \frac{dG}{dt} = fN - \theta_2 G + \phi GZ \end{cases} \quad (1)$$

With initial condition

$$N(0) = N_0 > 0, Z(0) = Z_0 > 0, O(0) = O_0 > 0, P(0) = P_0 > 0, T(0) = T_0 \geq 0, G(0) = G_0 > 0$$

Where; N(t) is the nutrient concentration at time t, Z(t) is the zooplankton biomass at time t, O(t) is the dissolved oxygen concentration at time t, P(t) is the phytoplankton biomass at time t, T(t) is the temperature of the upper ocean at time t, and G(t) is the greenhouse gas concentration at time t.

Lemma: For the system $\frac{dl}{dt} = g(l), l_e = 0$ a Lyapunov function candidate is chosen as $V(l) = g(l)^T Bg(l)$. The sufficient condition for asymptotic stability is that there exists a symmetric positive definite matrix *B* such that;

$$A(l)^T B + BA(l) = -Q(l) < 0, \forall x \in N \text{ (a neighborhood of 0)}$$

Where $A(l) = \frac{\partial g(l)}{\partial l}$ is the Jacobian matrix of $g(l)$, $l = N, Z, O, P, T, G$, and B is an identity matrix.

If the condition holds for all $l \in R^6$ and, additionally, $V(l)$ is radially unbounded, then it is globally asymptotically stable.

Proof:

Let

$$\begin{cases} g_1 = D(N_0 - N) - \alpha NP + m_1 d_1 P(t-\tau_1) + m_2 d_2 Z(t-\tau_2) - \sigma NT \\ g_2 = \frac{k_2 \beta PZ}{a+P} - \frac{k_3 \beta ZP(t-\tau_3)}{a+P(t-\tau_3)} - (D+d_2)Z - \varepsilon TZ - \phi GZ \\ g_3 = \psi P - \mu TO - \delta wO - \pi_1 PO - \pi_2 ZO - \pi_3 GO \\ g_4 = k_1 \alpha NP - (D+d_1)P - \frac{\beta PZ}{a+P} - vP^2 - hTP + \pi_1 PO \\ g_5 = \theta_1 GT + \sigma NT - xT + \varepsilon TZ \\ g_6 = fN - \theta_2 G + \phi GZ \end{cases} \quad (2)$$

ISSN No. 2321-2705 | DOI: 10.51244/IJRSI |Volume XIII Issue VI June 2026

Such that;

$$\frac{dl}{dt}=g(l)=\begin{bmatrix} g_1(l) \\ g_2(l) \\ g_3(l) \\ g_4(l) \\ g_5(l) \\ g_6(l) \end{bmatrix} \text{ and } g(l)^T=\left[g_1(l)+g_2(l)+g_3(l)+g_4(l)+g_5(l)+g_6(l)\right] \quad (3)$$

Where $l=N,Z,O,P,T,G$, and B is an identity matrix.

Then a Lyapunov function candidate is chosen as;

$$V(l)=g((l))^T Bg((l))=\left(g_1(l)\right)^2+\left(g_2(l)\right)^2+\left(g_3(l)\right)^2+\left(g_4(l)\right)^2+\left(g_5(l)\right)^2+\left(g_6(l)\right)^2 \quad (4)$$
$$=\|l\|^2$$

Therefore;

$$\frac{dl}{dt}=g(l)=\begin{bmatrix} D(N_0-N)-\alpha NP+m_1d_1P(\mathrm{t}-\tau_1)+m_2d_2Z(\mathrm{t}-\tau_2)-\sigma NT \\ \frac{k_2\beta PZ}{a+P}-\frac{k_3\beta ZP(\mathrm{t}-\tau_3)}{a+P(\mathrm{t}-\tau_3)}-(D+d_2)Z-\varepsilon TZ-\phi GZ \\ \psi P-\mu TO-\delta wO-\pi_1PO-\pi_2ZO-\pi_3GO \\ k_1\alpha NP-(D+d_1)P-\frac{\beta PZ}{a+P}-vP^2-hTP+\pi_1PO \\ \theta_1GT+\sigma NT-xT+\varepsilon TZ \\ fN-\theta_2G+\phi GZ \end{bmatrix}, \quad (5)$$

and

$$g(l)^T=\begin{bmatrix} D(N_0-N) & \frac{k_2\beta PZ}{a+P} & & k_1\alpha NP- & & \\ -\alpha NP & & \psi P-\mu TO & (D+d_1)P & & \\ +m_1d_1P(\mathrm{t}-\tau_1) & -\frac{k_3\beta ZP(\mathrm{t}-\tau_3)}{a+P(\mathrm{t}-\tau_3)} & -\delta wO-\pi_1PO & -\frac{\beta PZ}{a+P}- & \theta_1GT+\sigma NT & fN-\theta_2G \\ +m_2d_2Z(\mathrm{t}-\tau_2) & -(D+d_2)Z & -\pi_2ZO-\pi_3GO & vP^2-hTP & -xT+\varepsilon TZ & +\phi GZ \\ -\sigma NT & -\varepsilon TZ-\phi GZ & & +\pi_1PO & & \end{bmatrix} \quad (6)$$

Thus;

$$V(l)=\left[D(N_0-N)-\alpha NP+m_1d_1P(\mathrm{t}-\tau_1)+m_2d_2Z(\mathrm{t}-\tau_2)-\sigma NT\right]^2+\begin{bmatrix} \frac{k_2\beta PZ}{a+P}-\frac{k_3\beta ZP(\mathrm{t}-\tau_3)}{a+P(\mathrm{t}-\tau_3)} \\ -(D+d_2)Z-\varepsilon TZ-\phi GZ \end{bmatrix}^2$$
$$+\left[\psi P-\mu TO-\delta wO-\pi_1PO-\pi_2ZO-\pi_3GO\right]^2+\left[k_1\alpha NP-(D+d_1)P-\frac{\beta PZ}{a+P}-vP^2-hTP+\pi_1PO\right]^2$$
$$+\left[\theta_1GT+\sigma NT-xT+\varepsilon TZ\right]^2+\left[fN-\theta_2G+\phi GZ\right]^2$$

And

To prove $A(l)^T B+BA(l)=-Q(l)<0$ we maintain the variables define in equation (2). Therefore, we let

ISSN No. 2321-2705 | DOI: 10.51244/IJRSI |Volume XIII Issue VI June 2026

$$J(E_0)=\begin{vmatrix} A_1 & 0 & 0 & -A_2 & -A_3 & 0 \\ 0 & A_4 & 0 & A_5 & -A_6 & -A_7 \\ 0 & -A_8 & A_9 & A_{10} & -A_{11} & -A_{12} \\ A_{13} & A_{14} & A_{15} & A_{16} & -A_{17} & 0 \\ A_{18} & A_{19} & 0 & 0 & A_{20} & A_{21} \\ f & A_{22} & 0 & 0 & 0 & A_{23} \end{vmatrix} = A(l) \qquad (7)$$

Where;

$$A_1 = -D + \alpha\left(\frac{av - k_1\alpha N + D + d_1 - \pi_1 O + hT \pm \sqrt{\left(av + k_1\alpha N - D - d_1 + \pi_1 O - hT\right)^2 - 4v\beta Z}}{2v}\right)$$

$$-\left(\frac{\sigma D N_0 + m_1 d_1 P(t-\tau_1) + m_2 d_2 Z(t-\tau_2)}{x - \varepsilon Z - \theta_1 G} - D - \alpha P\right),$$

$$A_2 = \frac{\alpha\left(DN_0 + m_1 d_1 P(t-\tau_1) + m_2 d_2 Z(t-\tau_2)\right)}{D + \alpha P + \sigma T}, A_3 = \frac{\sigma\left(DN_0 + m_1 d_1 P(t-\tau_1) + m_2 d_2 Z(t-\tau_2)\right)}{D + \alpha P + \sigma T}$$

$$A_4 = k_2\beta\left(\frac{-\left(av - k_1\alpha N + D + d_1 - \pi_1 O + hT\right) \pm \sqrt{\left(av + k_1\alpha N - D - d_1 + \pi_1 O - hT\right)^2 - 4v\beta Z}}{2av - \left(av - k_1\alpha N + D + d_1 - \pi_1 O + hT\right) \pm \sqrt{\left(av + k_1\alpha N - D - d_1 + \pi_1 O - hT\right)^2 - 4v\beta Z}}\right)$$

$$-\frac{k_3\beta P(\mathrm{t}-\tau_3)}{a + P(\mathrm{t}-\tau_3)} - (D + d_2) - \frac{\varepsilon}{\sigma}\left(\frac{\sigma D N_0 + m_1 d_1 P(t-\tau_1) + m_2 d_2 Z(t-\tau_2)}{x - \varepsilon Z - \theta_1 G} - D - \alpha P\right) - \frac{\phi f N}{\theta_2 - \phi Z}$$

$$A_5 = \frac{k_2\beta a\left(\frac{\theta_2}{\phi} - \frac{fN\left(a+P\right)\left(a+P(t-\tau_3)\right)}{k_2\beta P - k_3\beta P(t-\tau_3) - \left(D + d_2 + \varepsilon T\right)\left(a+P\right)\left(a+P(t-\tau_3)\right)}\right)}{\left(a + \frac{-\left(av - k_1\alpha N + D + d_1 - \pi_1 O + hT\right) \pm \sqrt{\left(av + k_1\alpha N - D - d_1 + \pi_1 O - hT\right)^2 - 4v\beta Z}}{2v}\right)^2},$$

$$A_6 = \varepsilon\left(\frac{\theta_2}{\phi} - \frac{fN\left(a+P\right)\left(a+P(t-\tau_3)\right)}{k_2\beta P - k_3\beta P(t-\tau_3) - \left(D + d_2 + \varepsilon T\right)\left(a+P\right)\left(a+P(t-\tau_3)\right)}\right),$$

$$, A_7 = \phi\left(\frac{\theta_2}{\phi} - \frac{fN\left(a+P\right)\left(a+P(t-\tau_3)\right)}{k_2\beta P - k_3\beta P(t-\tau_3) - \left(D + d_2 + \varepsilon T\right)\left(a+P\right)\left(a+P(t-\tau_3)\right)}\right), A_8 = \frac{\pi_2\psi P}{\mu T + \delta w + \pi_1 P + \pi_2 Z + \pi_3 G},$$

$$A_9 = -\frac{\mu}{\sigma}\left(\frac{\sigma D N_0 + m_1 d_1 P(t-\tau_1) + m_2 d_2 Z(t-\tau_2)}{x - \varepsilon Z - \theta_1 G} - D - \alpha P\right) - \delta w - \frac{\pi_3 f N}{\theta_2 - \phi Z}$$

$$-\pi_1\left(\frac{-\left(av - k_1\alpha N + D + d_1 - \pi_1 O + hT\right) \pm \sqrt{\left(av + k_1\alpha N - D - d_1 + \pi_1 O - hT\right)^2 - 4v\beta Z}}{2v}\right)$$

ISSN No. 2321-2705 | DOI: 10.51244/IJRSI |Volume XIII Issue VI June 2026

$$-\pi_2\left(\frac{\theta_2}{\phi}-\frac{fN\left(a+P\right)\left(a+P(t-\tau_3)\right)}{k_2\beta P-k_3\beta P(t-\tau_3)-\left(D+d_2+\varepsilon T\right)\left(a+P\right)\left(a+P(t-\tau_3)\right)}\right)$$

$$A_{10}=\frac{\psi\left(\mu T+\delta w+\pi_2 Z+\pi_3 G\right)}{\mu T+\delta w+\pi_1 P+\pi_2 Z+\pi_3 G},\ A_{11}=\frac{\mu\psi P}{\mu T+\delta w+\pi_1 P+\pi_2 Z+\pi_3 G},\ A_{12}=\frac{\pi_3\psi P}{\mu T+\delta w+\pi_1 P+\pi_2 Z+\pi_3 G}$$

$$A_{13}=k_1\alpha\left(\frac{-\left(av-k_1\alpha N+D+d_1-\pi_1 O+hT\right)\pm\sqrt{\left(av+k_1\alpha N-D-d_1+\pi_1 O-hT\right)^2-4v\beta Z}}{2v}\right)$$

$$A_{14}=-\beta\left(\frac{-\left(av-k_1\alpha N+D+d_1-\pi_1 O+hT\right)\pm\sqrt{\left(av+k_1\alpha N-D-d_1+\pi_1 O-hT\right)^2-4v\beta Z}}{2av-\left(av-k_1\alpha N+D+d_1-\pi_1 O+hT\right)\pm\sqrt{\left(av+k_1\alpha N-D-d_1+\pi_1 O-hT\right)^2-4v\beta Z}}\right)$$

$$A_{15}=\pi_1\left(\frac{-\left(av-k_1\alpha N+D+d_1-\pi_1 O+hT\right)\pm\sqrt{\left(av+k_1\alpha N-D-d_1+\pi_1 O-hT\right)^2-4v\beta Z}}{2v}\right),$$

$$A_{16}=k_1\alpha\left(\frac{DN_0+m_1d_1P(t-\tau_1)+m_2d_2Z(t-\tau_2)}{D+\alpha P+\sigma T}\right)-(D+d_1)+\frac{\pi_1\psi P}{\mu T+\delta w+\pi_1 P+\pi_2 Z+\pi_3 G}$$

$$-\frac{\beta a\left(\frac{\theta_2}{\phi}-\frac{fN\left(a+P\right)\left(a+P(t-\tau_3)\right)}{k_2\beta P-k_3\beta P(t-\tau_3)-\left(D+d_2+\varepsilon T\right)\left(a+P\right)\left(a+P(t-\tau_3)\right)}\right)}{\left(a+\frac{-\left(av-k_1\alpha N+D+d_1-\pi_1 O+hT\right)\pm\sqrt{\left(av+k_1\alpha N-D-d_1+\pi_1 O-hT\right)^2-4v\beta Z}}{2v}\right)^2}$$

$$+\left(av-k_1\alpha N+D+d_1-\pi_1 O+hT\right)\pm\sqrt{\left(av+k_1\alpha N-D-d_1+\pi_1 O-hT\right)^2-4v\beta Z}$$

$$-\frac{h}{\sigma}\left(\frac{\sigma DN_0+m_1d_1P(t-\tau_1)+m_2d_2Z(t-\tau_2)}{x-\varepsilon Z-\theta_1 G}-D-\alpha P\right)$$

$$A_{17}=h\left(\frac{-\left(av-k_1\alpha N+D+d_1-\pi_1 O+hT\right)\pm\sqrt{\left(av+k_1\alpha N-D-d_1+\pi_1 O-hT\right)^2-4v\beta Z}}{2v}\right)$$

$$A_{18}=\frac{\sigma DN_0+m_1d_1P(t-\tau_1)+m_2d_2Z(t-\tau_2)}{x-\varepsilon Z-\theta_1 G}-D-\alpha P$$

$$A_{19}=\frac{\varepsilon}{\sigma}\left(\frac{\sigma DN_0+m_1d_1P(t-\tau_1)+m_2d_2Z(t-\tau_2)}{x-\varepsilon Z-\theta_1 G}-D-\alpha P\right)$$

$$A_{20}=\varepsilon\left(\frac{\theta_2}{\phi}-\frac{fN\left(a+P\right)\left(a+P(t-\tau_3)\right)}{k_2\beta P-k_3\beta P(t-\tau_3)-\left(D+d_2+\varepsilon T\right)\left(a+P\right)\left(a+P(t-\tau_3)\right)}\right)-x$$

$$+\frac{\theta_1 fN}{\theta_2-\phi Z}+\sigma\left(\frac{DN_0+m_1d_1P(t-\tau_1)+m_2d_2Z(t-\tau_2)}{D+\alpha P+\sigma T}\right)$$

$$A_{21}=\frac{\theta_1}{\sigma}\left(\frac{\sigma DN_0+m_1d_1P(t-\tau_1)+m_2d_2Z(t-\tau_2)}{x-\varepsilon Z-\theta_1 G}-D-\alpha P\right)$$

ISSN No. 2321-2705 | DOI: 10.51244/IJRSI |Volume XIII Issue VI June 2026

$$A_{22} = \frac{\phi f N}{\theta_2 - \phi Z}$$

$$A_{23} = -\theta_2 + \phi\left(\frac{\theta_2}{\phi} - \frac{fN\left(a+P\right)\left(a+P(t-\tau_3)\right)}{k_2\beta P - k_3\beta P(t-\tau_3) - \left(D+d_2+\varepsilon T\right)\left(a+P\right)\left(a+P(t-\tau_3)\right)}\right)$$

Where equation (7) is the Jacobian of the coexistence equilibrium point E_0.

So that;
$$A(l)^T = \begin{vmatrix} A_1 & 0 & 0 & A_{13} & A_{18} & f \\ 0 & A_4 & -A_8 & A_{14} & A_{19} & A_{22} \\ 0 & 0 & A_9 & A_{15} & 0 & 0 \\ -A_2 & A_5 & A_{10} & A_{16} & 0 & 0 \\ -A_3 & -A_6 & -A_{11} & -A_{17} & A_{20} & 0 \\ 0 & -A_7 & -A_{12} & 0 & A_{21} & A_{23} \end{vmatrix} \quad (8)$$

Then we show that; $A(l)^T + A(l) = -Q(l) < 0$

$$A(l)^T + A(l) = \begin{vmatrix} A_1 & 0 & 0 & A_{13} & A_{18} & f \\ 0 & A_4 & -A_8 & A_{14} & A_{19} & A_{22} \\ 0 & 0 & A_9 & A_{15} & 0 & 0 \\ -A_2 & A_5 & A_{10} & A_{16} & 0 & 0 \\ -A_3 & -A_6 & -A_{11} & -A_{17} & A_{20} & 0 \\ 0 & -A_7 & -A_{12} & 0 & A_{21} & A_{23} \end{vmatrix} + \begin{vmatrix} A_1 & 0 & 0 & -A_2 & -A_3 & 0 \\ 0 & A_4 & 0 & A_5 & -A_6 & -A_7 \\ 0 & -A_8 & A_9 & A_{10} & -A_{11} & -A_{12} \\ A_{13} & A_{14} & A_{15} & A_{16} & -A_{17} & 0 \\ A_{18} & A_{19} & 0 & 0 & A_{20} & A_{21} \\ f & A_{22} & 0 & 0 & 0 & A_{23} \end{vmatrix} \quad (9)$$

$$A(l)^T + A(l) = \begin{vmatrix} 2A_1 & 0 & 0 & A_{13}-A_2 & A_{18}-A_3 & f \\ 0 & 2A_4 & -A_8 & A_{14}+A_5 & A_{19}-A_6 & A_{22}-A_7 \\ 0 & -A_8 & 2A_9 & A_{15}+A_{10} & -A_{11} & -A_{12} \\ A_{13}-A_2 & A_5+A_{14} & A_{10}+A_{15} & 2A_{16} & -A_{17} & 0 \\ A_{18}-A_3 & A_{19}-A_6 & -A_{11} & -A_{17} & 2A_{20} & A_{21} \\ f & A_{22}-A_7 & -A_{12} & 0 & A_{21} & 2A_{23} \end{vmatrix} = -Q(l) \quad (10)$$

Thus;
$$Q(l) = -\begin{vmatrix} 2A_1 & 0 & 0 & A_{13}-A_2 & A_{18}-A_3 & f \\ 0 & 2A_4 & -A_8 & A_{14}+A_5 & A_{19}-A_6 & A_{22}-A_7 \\ 0 & -A_8 & 2A_9 & A_{15}+A_{10} & -A_{11} & -A_{12} \\ A_{13}-A_2 & A_5+A_{14} & A_{10}+A_{15} & 2A_{16} & -A_{17} & 0 \\ A_{18}-A_3 & A_{19}-A_6 & -A_{11} & -A_{17} & 2A_{20} & A_{21} \\ f & A_{22}-A_7 & -A_{12} & 0 & A_{21} & 2A_{23} \end{vmatrix} < 0 \quad (11)$$

$$Q(l) = \begin{vmatrix} -2A_1 & 0 & 0 & A_2-A_{13} & A_3-A_{18} & -f \\ 0 & -2A_4 & A_8 & -\left(A_{14}+A_5\right) & A_6-A_{19} & A_7-A_{22} \\ 0 & A_8 & -2A_9 & -\left(A_{15}+A_{10}\right) & A_{11} & A_{12} \\ A_2-A_{13} & -\left(A_5+A_{14}\right) & -\left(A_{10}+A_{15}\right) & -2A_{16} & A_{17} & 0 \\ A_3-A_{18} & A_6-A_{19} & A_{11} & A_{17} & -2A_{20} & -A_{21} \\ -f & A_7-A_{22} & A_{12} & 0 & -A_{21} & -2A_{23} \end{vmatrix} < 0 \quad (12)$$

ISSN No. 2321-2705 | DOI: 10.51244/IJRSI |Volume XIII Issue VI June 2026

$$Q(l)=\begin{vmatrix} Q_1 & 0 & 0 & Q_2 & Q_3 & -f \\ 0 & Q_4 & Q_5 & Q_6 & Q_7 & Q_8 \\ 0 & Q_9 & Q_{10} & Q_{11} & Q_{12} & Q_{13} \\ Q_{14} & Q_{15} & Q_{16} & Q_{17} & Q_{18} & 0 \\ Q_{19} & Q_{20} & Q_{21} & Q_{22} & Q_{23} & Q_{24} \\ -f & Q_{25} & Q_{26} & 0 & Q_{27} & Q_{28} \end{vmatrix} < 0 \qquad (13)$$

Thus, $A(l)^T + A(l) = -Q(l) < 0$.

Where; $\Delta = \left(av + k_1\alpha N - D - d_1 + \pi_1 O - hT\right)^2 - 4v\beta Z$

$$Q_1 = 2\left[\begin{array}{l} 2D - \alpha\left(\dfrac{av - k_1\alpha N + D + d_1 - \pi_1 O + hT \pm \sqrt{\Delta}}{2v}\right) \\ +\left(\dfrac{\sigma DN_0 + m_1 d_1 P(t-\tau_1) + m_2 d_2 Z(t-\tau_2)}{x - \varepsilon Z - \theta_1 G} + \alpha P\right) \end{array}\right],$$

$$Q_2 = \frac{\alpha\left(DN_0 + m_1 d_1 P(t-\tau_1) + m_2 d_2 Z(t-\tau_2)\right)}{D + \alpha P + \sigma T} - k_1\alpha\left(\frac{-\left(av - k_1\alpha N + D + d_1 - \pi_1 O + hT\right) \pm \sqrt{\Delta}}{2v}\right),$$

$$Q_3 = \frac{\sigma\left(DN_0 + m_1 d_1 P(t-\tau_1) + m_2 d_2 Z(t-\tau_2)\right)}{D + \alpha P + \sigma T} - \frac{\sigma DN_0 + m_1 d_1 P(t-\tau_1) + m_2 d_2 Z(t-\tau_2)}{x - \varepsilon Z - \theta_1 G} - D - \alpha P,$$

$$Q_4 = 2\left[\begin{array}{l} -k_2\beta\left(\dfrac{-\left(av - k_1\alpha N + D + d_1 - \pi_1 O + hT\right) \pm \sqrt{\Delta}}{2av - \left(av - k_1\alpha N + D + d_1 - \pi_1 O + hT\right) \pm \sqrt{\Delta}}\right) + \dfrac{k_3\beta P(\mathrm{t}-\tau_3)}{a + P(\mathrm{t}-\tau_3)} + (D + d_2) \\ +\dfrac{\varepsilon}{\sigma}\left(\dfrac{\sigma DN_0 + m_1 d_1 P(t-\tau_1) + m_2 d_2 Z(t-\tau_2)}{x - \varepsilon Z - \theta_1 G} - D - \alpha P\right) + \dfrac{\phi f N}{\theta_2 - \phi Z} \end{array}\right],$$

$$Q_5 = \frac{\pi_2 \psi P}{\mu T + \delta w + \pi_1 P + \pi_2 Z + \pi_3 G},$$

$$Q_6 = \beta\left(\frac{-\left(av - k_1\alpha N + D + d_1 - \pi_1 O + hT\right) \pm \sqrt{\Delta}}{2av - \left(av - k_1\alpha N + D + d_1 - \pi_1 O + hT\right) \pm \sqrt{\Delta}}\right)$$
$$- \frac{k_2\beta a\left(\dfrac{\theta_2}{\phi} - \dfrac{fN(a+P)\left(a + P(t-\tau_3)\right)}{k_2\beta P - k_3\beta P(t-\tau_3) - \left(D + d_2 + \varepsilon T\right)(a+P)\left(a + P(t-\tau_3)\right)}\right)}{\left(a + \dfrac{-\left(av - k_1\alpha N + D + d_1 - \pi_1 O + hT\right) \pm \sqrt{\Delta}}{2v}\right)^2},$$

$$Q_7 = \varepsilon\left(\frac{\theta_2}{\phi} - \frac{fN(a+P)\left(a + P(t-\tau_3)\right)}{k_2\beta P - k_3\beta P(t-\tau_3) - \left(D + d_2 + \varepsilon T\right)(a+P)\left(a + P(t-\tau_3)\right)}\right)$$
$$- \frac{\varepsilon}{\sigma}\left(\frac{\sigma DN_0 + m_1 d_1 P(t-\tau_1) + m_2 d_2 Z(t-\tau_2)}{x - \varepsilon Z - \theta_1 G} - D - \alpha P\right),$$

$$Q_8 = \phi\left(\frac{\theta_2}{\phi} - \frac{fN(a+P)\left(a + P(t-\tau_3)\right)}{k_2\beta P - k_3\beta P(t-\tau_3) - \left(D + d_2 + \varepsilon T\right)(a+P)\left(a + P(t-\tau_3)\right)}\right) - \frac{\phi f N}{\theta_2 - \phi Z},$$

ISSN No. 2321-2705 | DOI: 10.51244/IJRSI |Volume XIII Issue VI June 2026

$$Q_9 = \frac{\pi_2 \psi P}{\mu T + \delta w + \pi_1 P + \pi_2 Z + \pi_3 G},$$

$$Q_{10} = 2\left[\begin{array}{l} \frac{\mu}{\sigma}\left(\frac{\sigma D N_0 + m_1 d_1 P(t-\tau_1) + m_2 d_2 Z(t-\tau_2)}{x - \varepsilon Z - \theta_1 G} - D - \alpha P\right) + \delta w + \frac{\pi_3 f N}{\theta_2 - \phi Z} \\ + \pi_1\left(\frac{-\left(av - k_1 \alpha N + D + d_1 - \pi_1 O + hT\right) \pm \sqrt{\Delta}}{2v}\right) \\ + \pi_2\left(\frac{\theta_2}{\phi} - \frac{f N\left(a+P\right)\left(a+P(t-\tau_3)\right)}{k_2 \beta P - k_3 \beta P(t-\tau_3) - \left(D + d_2 + \varepsilon T\right)\left(a+P\right)\left(a+P(t-\tau_3)\right)}\right) \end{array}\right],$$

$$Q_{11} = -\frac{\psi\left(\mu T + \delta w + \pi_2 Z + \pi_3 G\right)}{\mu T + \delta w + \pi_1 P + \pi_2 Z + \pi_3 G} - \pi_1\left(\frac{-\left(av - k_1 \alpha N + D + d_1 - \pi_1 O + hT\right) \pm \sqrt{\Delta}}{2v}\right),$$

$$Q_{12} = \frac{\mu \psi P}{\mu T + \delta w + \pi_1 P + \pi_2 Z + \pi_3 G},$$

$$Q_{13} = \frac{\pi_3 \psi P}{\mu T + \delta w + \pi_1 P + \pi_2 Z + \pi_3 G},$$

$$Q_{14} = \frac{\alpha\left(D N_0 + m_1 d_1 P(t-\tau_1) + m_2 d_2 Z(t-\tau_2)\right)}{D + \alpha P + \sigma T} - k_1 \alpha\left(\frac{-\left(av - k_1 \alpha N + D + d_1 - \pi_1 O + hT\right) \pm \sqrt{\Delta}}{2v}\right),$$

$$Q_{15} = \beta\left(\frac{-\left(av - k_1 \alpha N + D + d_1 - \pi_1 O + hT\right) \pm \sqrt{\Delta}}{2av - \left(av - k_1 \alpha N + D + d_1 - \pi_1 O + hT\right) \pm \sqrt{\Delta}}\right)$$
$$- \frac{k_2 \beta a\left(\frac{\theta_2}{\phi} - \frac{f N\left(a+P\right)\left(a+P(t-\tau_3)\right)}{k_2 \beta P - k_3 \beta P(t-\tau_3) - \left(D + d_2 + \varepsilon T\right)\left(a+P\right)\left(a+P(t-\tau_3)\right)}\right)}{\left(a + \frac{-\left(av - k_1 \alpha N + D + d_1 - \pi_1 O + hT\right) \pm \sqrt{\Delta}}{2v}\right)^2}$$

$$Q_{16} = -\left[\frac{\psi\left(\mu T + \delta w + \pi_2 Z + \pi_3 G\right)}{\mu T + \delta w + \pi_1 P + \pi_2 Z + \pi_3 G} + \pi_1\left(\frac{-\left(av - k_1 \alpha N + D + d_1 - \pi_1 O + hT\right) \pm \sqrt{\Delta}}{2v}\right)\right],$$

$$Q_{17} = 2\left[\begin{array}{l} -k_1 \alpha\left(\frac{D N_0 + m_1 d_1 P(t-\tau_1) + m_2 d_2 Z(t-\tau_2)}{D + \alpha P + \sigma T}\right) + (D + d_1) - \frac{\pi_1 \psi P}{\mu T + \delta w + \pi_1 P + \pi_2 Z + \pi_3 G} \\ + \frac{\beta a\left(\frac{\theta_2}{\phi} - \frac{f N\left(a+P\right)\left(a+P(t-\tau_3)\right)}{k_2 \beta P - k_3 \beta P(t-\tau_3) - \left(D + d_2 + \varepsilon T\right)\left(a+P\right)\left(a+P(t-\tau_3)\right)}\right)}{\left(a + \frac{-\left(av - k_1 \alpha N + D + d_1 - \pi_1 O + hT\right) \pm \sqrt{\Delta}}{2v}\right)^2} \\ -\left(av - k_1 \alpha N + D + d_1 - \pi_1 O + hT\right) \pm \sqrt{\Delta} \\ + \frac{h}{\sigma}\left(\frac{\sigma D N_0 + m_1 d_1 P(t-\tau_1) + m_2 d_2 Z(t-\tau_2)}{x - \varepsilon Z - \theta_1 G} - D - \alpha P\right) \end{array}\right],$$

$$Q_{18} = h\left(\frac{-\left(av - k_1 \alpha N + D + d_1 - \pi_1 O + hT\right) \pm \sqrt{\Delta}}{2v}\right),$$

ISSN No. 2321-2705 | DOI: 10.51244/IJRSI |Volume XIII Issue VI June 2026

$$Q_{19} = Q_3 = \frac{\sigma\left(DN_0 + m_1 d_1 P(t-\tau_1) + m_2 d_2 Z(t-\tau_2)\right)}{D+\alpha P+\sigma T} - \frac{\sigma DN_0 + m_1 d_1 P(t-\tau_1) + m_2 d_2 Z(t-\tau_2)}{x-\varepsilon Z-\theta_1 G} - D - \alpha P,$$

$$Q_{20} = \varepsilon\left(\frac{\theta_2}{\phi} - \frac{fN\left(a+P\right)\left(a+P(t-\tau_3)\right)}{k_2\beta P - k_3\beta P(t-\tau_3) - \left(D+d_2+\varepsilon T\right)\left(a+P\right)\left(a+P(t-\tau_3)\right)}\right)$$

$$-\frac{\varepsilon}{\sigma}\left(\frac{\sigma DN_0 + m_1 d_1 P(t-\tau_1) + m_2 d_2 Z(t-\tau_2)}{x-\varepsilon Z-\theta_1 G} - D - \alpha P\right),$$

$$Q_{21} = \frac{\mu\psi P}{\mu T+\delta w+\pi_1 P+\pi_2 Z+\pi_3 G},$$

$$Q_{22} = h\left(\frac{-\left(av-k_1\alpha N+D+d_1-\pi_1 O+hT\right)\pm\sqrt{\Delta}}{2v}\right),$$

$$Q_{23} = 2\left[\begin{array}{l} x-\varepsilon\left(\dfrac{\theta_2}{\phi} - \dfrac{fN\left(a+P\right)\left(a+P(t-\tau_3)\right)}{k_2\beta P - k_3\beta P(t-\tau_3) - \left(D+d_2+\varepsilon T\right)\left(a+P\right)\left(a+P(t-\tau_3)\right)}\right) \\ -\dfrac{\theta_1 fN}{\theta_2-\phi Z} - \sigma\left(\dfrac{DN_0 + m_1 d_1 P(t-\tau_1) + m_2 d_2 Z(t-\tau_2)}{D+\alpha P+\sigma T}\right) \end{array}\right],$$

$$Q_{24} = -\frac{\theta_1}{\sigma}\left(\frac{\sigma DN_0 + m_1 d_1 P(t-\tau_1) + m_2 d_2 Z(t-\tau_2)}{x-\varepsilon Z-\theta_1 G} - D - \alpha P\right),$$

$$Q_{25} = \phi\left(\frac{\theta_2}{\phi} - \frac{fN\left(a+P\right)\left(a+P(t-\tau_3)\right)}{k_2\beta P - k_3\beta P(t-\tau_3) - \left(D+d_2+\varepsilon T\right)\left(a+P\right)\left(a+P(t-\tau_3)\right)}\right) - \frac{\phi fN}{\theta_2-\phi Z},$$

$$Q_{26} = \frac{\pi_3\psi P}{\mu T+\delta w+\pi_1 P+\pi_2 Z+\pi_3 G},$$

$$Q_{27} = -\frac{\theta_1}{\sigma}\left(\frac{\sigma DN_0 + m_1 d_1 P(t-\tau_1) + m_2 d_2 Z(t-\tau_2)}{x-\varepsilon Z-\theta_1 G} - D - \alpha P\right),$$

$$Q_{28} = 2\left[\theta_2 - \phi\left(\frac{\theta_2}{\phi} - \frac{fN\left(a+P\right)\left(a+P(t-\tau_3)\right)}{k_2\beta P - k_3\beta P(t-\tau_3) - \left(D+d_2+\varepsilon T\right)\left(a+P\right)\left(a+P(t-\tau_3)\right)}\right)\right]$$

Since $A(l)^T + A(l) = -Q(l) < 0$, $V(l) > 0$ **and** $V(l) \to \infty$ **as** $\|l\| \to \infty$ **(Where** $l = N, Z, O, P, T, G$**), therefore, the coexistence equilibrium point is globally asymptotically stable.**

Concentration Number

Motivated by the role of the basic reproduction number R_0 in epidemiological models as a threshold indicator of disease propagation, we introduce a related ecological metric known as the concentration number, denoted by C^*. C^* is the threshold for nutrient-driven phytoplankton amplification that serves as an early indicator of the potential for bloom-induced ocean deoxygenation. It characterizes the critical dissolved oxygen concentration at which the marine ecosystem transitions from a relatively stable state to one experiencing accelerated oxygen depletion. Values exceeding this threshold indicate increasing susceptibility to hypoxia and associated ecological disturbances, while lower values reflect conditions favorable for ecosystem persistence and recovery.

ISSN No. 2321-2705 | DOI: 10.51244/IJRSI |Volume XIII Issue VI June 2026

To determine the concentration number C^*, we adopt the next-generation matrix framework following the approach used in Achimugwu (2023) and Ochieng (2024). The model is decomposed into two components: a matrix F, which captures the production and propagation of deoxygenation-related effects, and V, which accounts for all other transitions, losses, and regulatory mechanisms. Following the next-generation matrix approach, the deoxygenation-free equilibrium is defined as the state in which the compartments responsible for propagating oxygen depletion vanish. Although nutrient concentration N(t), ocean upper temperature T(t), and greenhouse gas concentration G(t) are key environmental drivers of deoxygenation, they do not satisfy the requirements of deoxygenation-transmitting compartments because N(t) remains positive due to continuous external nutrient loading, N_0. Therefore, the ocean deoxygenation-free equilibrium is more appropriately characterized by the absence of the biologically active compartments involved in oxygen-depletion dynamics. These compartments are Z(t), O(t), and P(t). Thus, the reduced subsystem may be written in the standard form

$$\frac{dX}{dt} = F(X) - V(X) \tag{14}$$

Where $X = (Z, O, P)^T$. The threshold quantity C^* is subsequently obtained from the spectral radius of the matrix product FV^{-1}

Table 1: Parameter values

Parameter	Description	Values	Literature Source
D	Washout rate	$0.4\left(1day^{-1}\right)$	Macdonald & Gulbudak (2023)
w	Microbial decomposition efficiency factor	0.4	Chowdhury *et al.* (2024)
N_0	Constant input of nutrient concentration	$40\left(mgdm^{-3}\right)$	Rehim *et al.* (2016)
a	Half-saturation constant	$1.0\left(mgdm^{-3}\right)$	Rehim *et al.* (2016)
x	Temperature decrease rate	$0.1\ \left(day^{-1}\right)$	Assumed
v	Self-shading	0.02 $\left(\left(mgdm^{-3}\right)^{-1} day^{-1}\right)$	Rehim *et al.* (2016)
k_1	Conversion factor from nutrient to phytoplankton	0.5	Macdonald & Gulbudak (2023)
k_2	Conversion factor from phytoplankton to zooplankton	0.4	Rehim *et al.* (2016)
k_3	Toxic substance production rate	$0.2\left(day^{-1}\right)$	Rehim *et al.* (2016)
f	Greenhouse gas increase rate	$0.05\left(day^{-1}\right)$	Assumed
m_1	Nutrient production from phytoplankton mortality	0.3	Rehim *et al.* (2016)
m_2	Nutrient production from zooplankton mortality	0.25	Rehim *et al.* (2016)
d_1	Natural mortality rate of phytoplankton	$0.1\left(day^{-1}\right)$	Rehim *et al.* (2016)

ISSN No. 2321-2705 | DOI: 10.51244/IJRSI |Volume XIII Issue VI June 2026

d_2	Natural mortality rate of zooplankton	$0.08\left(day^{-1}\right)$	Rehim *et al.* (2016)
h	Temperature inhibition rate	$0.03\ \left(day^{-1}\right)$	Roy et al. (2012)
ε	Temperature production rate	$0.01\ \left(day^{-1}\right)$	Assumed
α	Nutrient uptake rate	$0.4\left(1day^{-1}\right)$	Rehim *et al.* (2016)
ϕ	Greenhouse production rate	$0.012\ \left(day^{-1}\right)$	Assumed
β	Maximum zooplankton ingestion rate	$0.6\left(1day^{-1}\right)$	Rehim *et al.* (2016)
δ	Oxygen consumption by decomposition	$0.03\ \left(day^{-1}\right)$	Chowdhury *et al.* (2023)
ψ	Oxygen production by photosynthesis	$0.5\ \left(day^{-1}\right)$	Assumed
μ	Oxygen depletion due to temperature	$0.02\ \left(day^{-1}\right)$	Assumed
π_1	Oxygen consumption by phytoplankton respiration	$0.01\ \left(\left(mgdm^{-3}\right)^{-1} day^{-1}\right)$	Assumed
π_2	Oxygen consumption by zooplankton respiration	$0.015\ \left(\left(mgdm^{-3}\right)^{-1} day^{-1}\right)$	Assumed
π_3	Oxygen depletion due to greenhouse gases	$0.01\left(day^{-1}\right)$	Assumed
σ	Nutrient depletion due to temperature	$0.04\ \left(day^{-1}\right)$	Assumed
θ_1	Temperature increase due to greenhouse gases	$0.025\ \left(day^{-1}\right)$	Assumed
θ_2	Greenhouse gas removal rate	$0.2\ \left(day^{-1}\right)$	Assumed
τ_1	Delay in phytoplankton decomposition	2.5 (days)	Rehim *et al.* (2016)
τ_2	Delay in zooplankton decomposition	4.0 (days)	Rehim *et al.* (2016)
τ_3	Delay for toxic-phytoplankton maturity	5.5 (days)	Rehim *et al.* (2016)

Here is the parameter table formatted for direct insertion into Microsoft Word (you can copy and paste it; Word will preserve it as a table in most cases).

Several model parameters ($x, f, \varepsilon, \phi, \psi, \mu, \pi_1, \pi_2, \pi_3, \sigma, \theta_1, \theta_2$) were assigned biologically plausible values because direct field measurements for these processes are currently unavailable. The assumed parameter values were intentionally chosen to satisfy three criteria:

1. they remain within biologically realistic orders of magnitude reported for marine ecosystem models;
2. they preserve positivity and boundedness of the model solutions; and
3. they reproduce ecologically realistic dynamics, including phytoplankton blooms, zooplankton persistence, and progressive oxygen depletion under climate-change forcing.

ISSN No. 2321-2705 | DOI: 10.51244/IJRSI |Volume XIII Issue VI June 2026

3.1 Existence of ocean deoxygenation-free equilibrium point

At equilibrium,

$$\frac{dN}{dt}=\frac{dZ}{dt}=\frac{dO}{dt}=\frac{dP}{dt}=\frac{dT}{dt}=\frac{dG}{dt}=0 \tag{15}$$

Thus, the system of equation becomes;

$$D(N_0-N)-\alpha NP+m_1d_1P(t-\tau_1)+m_2d_2Z(t-\tau_2)-\sigma NT=0 \tag{16}$$

$$\frac{k_2\beta PZ}{a+P}-\frac{k_3\beta ZP(t-\tau_3)}{a+P(t-\tau_3)}-(D+d_2)Z-\varepsilon TZ-\phi GZ=0 \tag{17}$$

$$\psi P-\mu TO-\delta wO-\pi_1PO-\pi_2ZO-\pi_3GO=0 \tag{18}$$

$$k_1\alpha NP-(D+d_1)P-\frac{\beta PZ}{a+P}-vP^2-hTP+\pi_1PO=0 \tag{19}$$

$$\theta_1GT+\sigma NT-xT+\varepsilon TZ=0 \tag{20}$$

$$fN-\theta_2G+\phi GZ=0 \tag{21}$$

When $Z=O=P=0$ we substitute into equations (16) – (21) to solve for N^*,Z^*,O^*,P^*,T^*,G^*, respectively.

$$N^*=\frac{DN_0}{D+\sigma T} \tag{22}$$

$$G^*=\frac{fN}{\theta_2} \tag{23}$$

Thus, the ocean deoxygenation-free equilibrium point $E_2=\left(N^*,Z^*,O^*,P^*,T^*,G^*\right)$. This gives

$$E_2=\left(\frac{DN_0}{D+\sigma T},0,0,0,0,\frac{fN}{\theta_2}\right). \tag{24}$$

Therefore, for $X=(Z,O,P)^T$, using the next generation matrix, we have;

$$F(X)=\begin{pmatrix}\frac{k_2\beta PZ}{a+P}\\ \psi P\\ k_1\alpha NP+\pi_1PO\end{pmatrix} \text{ and } V(X)=\begin{pmatrix}\frac{k_3\beta ZP(t-\tau_3)}{a+P(t-\tau_3)}+(D+d_2)Z+\varepsilon TZ+\phi GZ\\ \mu TO+\delta wO+\pi_1PO+\pi_2ZO+\pi_3GO\\ (D+d_1)P+\frac{\beta PZ}{a+P}+vP^2+hTP\end{pmatrix}$$

Let

$$f_1=\frac{k_2\beta PZ}{a+P},\qquad v_1=\frac{k_3\beta ZP(t-\tau_3)}{a+P(t-\tau_3)}+(D+d_2)Z+\varepsilon TZ+\phi GZ$$
$$f_2=\psi P,\qquad \text{, and } v_2=\mu TO+\delta wO+\pi_1PO+\pi_2ZO+\pi_3GO$$
$$f_3=k_1\alpha NP+\pi_1PO\qquad v_3=(D+d_1)P+\frac{\beta PZ}{a+P}+vP^2+hTP$$

Let the Jacobian matrices $F(X)$ and $V(X)$ be defined as:

ISSN No. 2321-2705 | DOI: 10.51244/IJRSI |Volume XIII Issue VI June 2026

$$F(X)=\begin{pmatrix} \frac{\partial f_1}{\partial Z} & \frac{\partial f_1}{\partial O} & \frac{\partial f_1}{\partial P} \\ \frac{\partial f_2}{\partial Z} & \frac{\partial f_2}{\partial O} & \frac{\partial f_2}{\partial P} \\ \frac{\partial f_3}{\partial Z} & \frac{\partial f_3}{\partial O} & \frac{\partial f_3}{\partial P} \end{pmatrix} \text{ and } V(X)=\begin{pmatrix} \frac{\partial v_1}{\partial Z} & \frac{\partial v_1}{\partial O} & \frac{\partial v_1}{\partial P} \\ \frac{\partial v_2}{\partial Z} & \frac{\partial v_2}{\partial O} & \frac{\partial v_2}{\partial P} \\ \frac{\partial v_3}{\partial Z} & \frac{\partial v_3}{\partial O} & \frac{\partial v_3}{\partial P} \end{pmatrix} \tag{25}$$

$$F(X)=\begin{pmatrix} \frac{k_2\beta P^*}{a+P^*} & 0 & \frac{k_2\beta Z^* a}{\left(a+P^*\right)^2} \\ 0 & 0 & \psi \\ 0 & \pi_1 P^* & k_1\alpha N^*+\pi_1 O^* \end{pmatrix} \tag{26}$$

$$V(X)=\begin{pmatrix} \frac{k_3\beta P^*(t-\tau_3)}{a+P^*(t-\tau_3)}+D+d_2+\varepsilon T^*+\phi G^* & 0 & 0 \\ \pi_2 O^* & \mu T^*+\delta w+\pi_1 P^*+\pi_2 Z^*+\pi_3 G^* & \pi_1 O^* \\ \frac{\beta P^*}{a+P^*} & 0 & D+d_1+\frac{\beta Z a}{\left(a+P^*\right)^2}+2vP^*+hT^* \end{pmatrix} \tag{27}$$

Evaluating $F(X)$ and $V(X)$ at equilibrium point E_2 yields

$$F(X)=\begin{pmatrix} 0 & 0 & 0 \\ 0 & 0 & \psi \\ 0 & 0 & k_1\alpha\frac{DN_0}{D+\sigma T} \end{pmatrix} \tag{28}$$

$$V(X)=\begin{pmatrix} D+d_2+\phi\frac{fN}{\theta_2} & 0 & 0 \\ 0 & \delta w+\pi_3\frac{fN}{\theta_2} & 0 \\ 0 & 0 & D+d_1 \end{pmatrix}$$

$$V(X)=\begin{pmatrix} \frac{\theta_2\left(D+d_2\right)+\phi fN}{\theta_2} & 0 & 0 \\ 0 & \frac{\theta_2\delta w+\pi_3 fN}{\theta_2} & 0 \\ 0 & 0 & D+d_1 \end{pmatrix} \tag{29}$$

$$V^{-1}=\begin{pmatrix} \frac{\theta_2}{\theta_2\left(D+d_2\right)+\phi fN} & 0 & 0 \\ 0 & \frac{\theta_2}{\theta_2\delta w+\pi_3 fN} & 0 \\ 0 & 0 & \frac{1}{D+d_1} \end{pmatrix} \tag{30}$$

Thus,

ISSN No. 2321-2705 | DOI: 10.51244/IJRSI |Volume XIII Issue VI June 2026

$$FV^{-1} = \begin{pmatrix} 0 & 0 & 0 \\ 0 & 0 & \psi \\ 0 & 0 & k_1\alpha\dfrac{DN_0}{D+\sigma T} \end{pmatrix} \begin{pmatrix} \dfrac{\theta_2}{\theta_2(D+d_2)+\phi fN} & 0 & 0 \\ 0 & \dfrac{\theta_2}{\theta_2\delta w+\pi_3 fN} & 0 \\ 0 & 0 & \dfrac{1}{D+d_1} \end{pmatrix}$$

$$FV^{-1} = \begin{pmatrix} 0 & 0 & 0 \\ 0 & 0 & \dfrac{\psi}{D+d_1} \\ 0 & 0 & \dfrac{k_1\alpha DN_0}{(D+\sigma T)(D+d_1)} \end{pmatrix} \tag{31}$$

$$|FV^{-1}-\lambda I| = \begin{vmatrix} -\lambda & 0 & 0 \\ 0 & -\lambda & \dfrac{\psi}{D+d_1} \\ 0 & 0 & \dfrac{k_1\alpha DN_0}{(D+\sigma T)(D+d_1)}-\lambda \end{vmatrix} = 0 \tag{32}$$

where I is an identity matrix of same size as (31). Hence, the eigenvalues of (32) are:

$\lambda_1 = 0, \lambda_2 = 0,$ and $\lambda_3 = \dfrac{k_1\alpha DN_0}{(D+\sigma T)(D+d_1)}$.

But $T = 0$. Thus,

$$\lambda_3 = \frac{k_1\alpha N_0}{D+d_1} \tag{33}$$

The concentration number, C^* is thus the spectral radius of (33) i.e

$$C^* = |FV^{-1}-\lambda I| = \max(|\lambda_1|,|\lambda_2|,|\lambda_3|) = |\lambda_3|$$

$$= \frac{k_1\alpha N_0}{D+d_1} \tag{34}$$

C^* quantifies the ability of nutrient-supported phytoplankton growth to overcome losses due to washout and natural mortality. When $C^* < 1$, the ocean deoxygenation-free equilibrium remains stable, indicating that phytoplankton biomass cannot accumulate sufficiently to trigger substantial oxygen depletion. Conversely, when $C^* > 1$, phytoplankton production exceeds removal, promoting bloom formation, increased organic matter decomposition, and intensified oxygen consumption. In this case, the marine ecosystem becomes vulnerable to persistent deoxygenation, and the deoxygenation-free state can no longer be maintained.

ISSN No. 2321-2705 | DOI: 10.51244/IJRSI |Volume XIII Issue VI June 2026

SENSITIVITY ANALYSIS

Sensitivity analysis is a valuable technique used to evaluate how variations in model parameters influence the behavior and predictions of a mathematical model. It provides insight into which parameters exert the strongest influence on the model outputs and therefore play the most significant role in determining system dynamics. In this study, the normalized sensitivity index of a parameter n with respect to the concentration number C^* measures the proportional change in C^* resulting from a proportional change in n. It is computed as:

$$S_n = \frac{n}{C^*}\frac{\partial C^*}{\partial n} \tag{35}$$

A positive sensitivity index S_n indicates that increasing the value of the parameter m leads to an increase in the concentration number C^*, whereas a negative index S_n implies that an increase in the parameter causes the concentration number to decrease. The magnitude of the sensitivity index reflects the strength of the parameter's influence on C^*; larger absolute values correspond to greater impact. Consequently, parameters associated with high sensitivity values are often regarded as key drivers of system behavior and are important targets for monitoring, management, or intervention strategies.

The parameters in the concentration number given by (19) are: k_1, α, N_0, D, d_1 .Using formula (35), the sensitivity indices are given by

$$S_{k_1} = \frac{k_1}{C^*}\frac{\partial C^*}{\partial k_1}, S_\alpha = \frac{\alpha}{C^*}\frac{\partial C^*}{\partial \alpha}, S_{N_0} = \frac{N_0}{C^*}\frac{\partial C^*}{\partial N_0}, S_D = \frac{D}{C^*}\frac{\partial C^*}{\partial D}, S_{d_1} = \frac{d_1}{C^*}\frac{\partial C^*}{\partial d_1} \tag{36}$$

Thus,

$$S_{k_1} = 1, S_\alpha = 1, S_{N_0} = 1, S_D = -\frac{D}{D+d_1}, S_{d_1} = -\frac{d_1}{D+d_1} \tag{37}$$

Using the parameters values in table 1 and substituting in (37), we have

$$C^* = 16\,,\, S_{k_1} = 1, S_\alpha = 1, S_{N_0} = 1, S_D = -0.8, S_{d_1} = -0.2 \tag{38}$$

Table 2: Sensitivity indices of the model parameters on the concentration number

Parameter	Description	Sensitivity index
k_1	Conversion factor from nutrient to phytoplankton	+1.0000
α	Nutrient uptake rate	+1.0000
N_0	Constant input of nutrient concentration	+1.0000
D	Washout rate	-0.8000
d_1	Natural mortality rate of phytoplankton	-0.2000

Therefore, parameters with positive sensitivity indices contribute to an increase in the nutrient-driven phytoplankton amplification that serves as an early indicator of the potential for bloom-induced ocean deoxygenation. And reducing their values can help lower bloom-induced ocean deoxygenation. In contrast, parameters with negative sensitivity indices act in the opposite direction, so increasing their values may help mitigate the bloom-induced ocean deoxygenation.

ISSN No. 2321-2705 | DOI: 10.51244/IJRSI |Volume XIII Issue VI June 2026

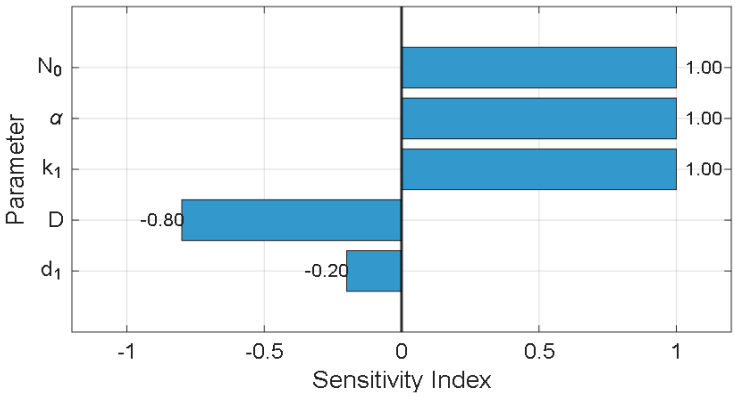

Figure 1: Tornado plot of sensitivity indices for the climate model

5.0 RESULTS AND DISCUSSION

This section discusses the main findings of the model analysis and examines their implications for ocean deoxygenation and climate-driven changes in marine ecosystems.

5.1 Global Stability of the Coexistence Equilibrium

From the analysis, we established that the Lyapunov functional is positive definite and radially unbounded, while its derivative along the trajectories of the system is strictly negative definite. Consequently, the coexistence equilibrium satisfies the conditions for global asymptotic stability.

This result implies that all model variables converge to a unique equilibrium state irrespective of the initial population densities or environmental conditions. From a biological perspective, the marine ecosystem possesses an intrinsic self-regulating mechanism capable of restoring equilibrium following environmental disturbances. Such behavior is particularly important in marine ecosystems subjected to increasing anthropogenic pressures, including nutrient enrichment, greenhouse gas accumulation, ocean warming, and oxygen depletion.

5.1.1 Ecological Implications for Ocean Deoxygenation

One of the most important outcomes of the global stability analysis is the persistence of dissolved oxygen within the ecosystem. The oxygen equation incorporates oxygen production through phytoplankton photosynthesis at rate ψ=0.5 day^{-1} and oxygen losses through microbial decomposition, respiration, greenhouse gas effects, and temperature-induced depletion.

The stability result indicates that oxygen-generating processes remain sufficiently strong to balance oxygen-consuming processes under the parameter regime considered. Consequently, dissolved oxygen does not decline indefinitely but approaches a stable equilibrium level. This finding suggests that the modeled ecosystem exhibits resilience against moderate deoxygenation pressures and can maintain ecological functionality despite environmental stress.

The result is ecologically meaningful because ocean deoxygenation has emerged as one of the most serious threats to marine biodiversity. Reduced oxygen concentrations alter species distributions, disrupt food-web interactions, and increase mortality among oxygen-sensitive organisms. Our model demonstrates that when nutrient recycling, plankton growth, and oxygen production remain active, the ecosystem can compensate for oxygen losses and recover towards a stable state.

5.1.2 Effects of Climate Warming and Greenhouse Gases

The model explicitly incorporates climate-related variables through the temperature and greenhouse gas compartments. Greenhouse gases increase ocean temperature through the parameter $\theta_1 = 0.025$, while increase temperature contributes to oxygen depletion and affects plankton dynamics. Conversely, greenhouse gases are removed at rate $\theta_2 = 0.2 day^{-1}$.

ISSN No. 2321-2705 | DOI: 10.51244/IJRSI |Volume XIII Issue VI June 2026

The global stability result demonstrates that the warming effects generated by greenhouse gases are insufficient to destabilize the ecosystem under the adopted parameter values. Although elevated temperatures increase biological oxygen demand and intensify oxygen depletion, the compensatory effects of nutrient cycling, phytoplankton productivity, and greenhouse gas removal maintain ecosystem stability. This indicates that the marine ecosystem can tolerate moderate climatic disturbances without undergoing irreversible degradation.

However, the result should not be interpreted as evidence that ocean warming is harmless. Instead, it indicates that the chosen parameter regime lies within a resilience threshold beyond which stability may no longer be guaranteed. Significant increases in temperature-dependent oxygen depletion μ, greenhouse gas production ϕ, or nutrient stress σ could potentially shift the system toward more severe deoxygenation states.

5.1.3 Significance of Time Delays

The model incorporates three biologically realistic delays representing phytoplankton decomposition ($\tau_1 = 2.5$ days), zooplankton decomposition ($\tau_2 = 4.0$ days), and toxic-phytoplankton maturation (τ_3=5.5 days).

The global stability result confirms that these delays do not destabilize the ecosystem under the considered conditions. This finding suggests that delayed nutrient recycling and delayed toxin production are adequately absorbed by the ecosystem's regulatory mechanisms. Ecologically, the result implies that natural lags in decomposition and biological maturation processes do not necessarily lead to persistent oscillations or ecosystem collapse when stabilizing feedbacks remain sufficiently strong.

5.2 Concentration number and its impact

The concentration number proposed in this study provides a dimensionless ecological threshold that quantifies the ability of nutrient-supported phytoplankton production to overcome biological and hydrodynamic loss processes. Unlike empirical environmental indicators, which measure the current state of an ecosystem, the concentration number characterizes the intrinsic capacity of the ecosystem to initiate and sustain phytoplankton proliferation under prevailing environmental conditions. Consequently, it serves as a mechanistic indicator of ecological resilience and bloom potential. For our proposed model,

$$C^* = \frac{k_1 \alpha N_0}{D + d_1}$$

where the numerator represents the effective production of phytoplankton resulting from nutrient availability and nutrient uptake efficiency, while the denominator represents phytoplankton removal through hydrodynamic flushing and natural mortality. Therefore, the concentration number compares the ecological production capacity of the phytoplankton community with its overall loss capacity.

$C^* = 16$ means the potential rate of phytoplankton production is sixteen times greater than the combined rate of phytoplankton removal through flushing and natural mortality. Equivalently,

$k_1 \alpha N_0 = 16(D + d_1)$.

Hence,

$k_1 \alpha N_0 \gg D + d_1$.

This indicates a strong dominance of phytoplankton growth over loss processes. This indicates that the ecological conditions necessary for bloom formation already exist. Large phytoplankton blooms subsequently produce large quantities of organic matter. When this biomass dies; bacteria decompose it, respiration increases, dissolved oxygen is consumed, hypoxia becomes increasingly likely.

ISSN No. 2321-2705 | DOI: 10.51244/IJRSI |Volume XIII Issue VI June 2026

While Achimugwu *et al.* (2023) introduced the concentration number as an environmental analogue of the basic reproduction number to quantify the persistence of excessive atmospheric carbon dioxide. Their model describes interactions among atmospheric carbon dioxide, photosynthetic biomass, conservation policies, environmental enlightenment, and direct air-capture technology. Consequently, their concentration number measures the balance between carbon dioxide accumulation and mitigation processes, with $C^* > 1$ indicating that atmospheric CO_2 accumulates faster than it can be removed by natural and technological control measures. Ochieng (2024) adopted the same threshold concept within a data-driven climate model calibrated using historical climate observations.

His model incorporated atmospheric carbon dioxide, photosynthetic biomass, human population density, and atmospheric temperature to predict future climate trends. In contrast to Achimugwu *et al.* (2023), where the concentration number evaluates mitigation effectiveness, Ochieng (2024) employed the threshold within a predictive framework to analyze long-term climate evolution under observed environmental conditions. Our study extends this threshold theory from atmospheric climate systems to marine ecosystem dynamics under ocean deoxygenation. Unlike the previous studies, where atmospheric carbon dioxide is the principal state variable, the proposed concentration number is derived from the nutrient–phytoplankton subsystem and quantifies the capacity of nutrient availability to sustain phytoplankton growth relative to phytoplankton losses through washout and natural mortality.

5.2.1 Sensitivity Indices of Model Parameters

A sensitivity analysis was performed to evaluate the effect of individual model parameters on the concentration number C^*, which serves as a threshold measure of bloom-induced ocean deoxygenation. The sensitivity indices were computed using the corresponding analytical expressions and parameter values listed in Table 1. The resulting indices are summarized in Table 2 and illustrated in Fig. 1.

The sensitivity analysis revealed that the concentration number, $C^* = 16$, is most strongly influenced by the nutrient-to-phytoplankton conversion coefficient k_1, phytoplankton growth rate α, and external nutrient concentration N_0; each exhibiting a normalized sensitivity index of +1.0. This indicates that proportional changes in any of these parameters produce equivalent proportional changes in the concentration number. Specifically, a 30% increase in k_1, α, and N_0 results in a 13% increase in C^*, thereby enhancing the likelihood and intensity of ocean deoxygenation. Conversely, the washout rate D and phytoplankton mortality rate d_1 possess negative sensitivity indices of -0.8 and -0.2, respectively. Specifically, a 30% increase in D and d_1 results in a 23.1% decrease in C^*. Implying that increases in these parameters suppress the concentration number and consequently reduce deoxygenation potential. The larger magnitude of the sensitivity index associated with D suggests that washout processes exert a stronger mitigating effect than phytoplankton mortality. Overall, the results identify nutrient enrichment, phytoplankton productivity, and biomass conversion efficiency as the dominant drivers of deoxygenation dynamics, while washout and mortality mechanisms act as important regulatory processes that enhance ecosystem resilience against oxygen depletion.

CONCLUSION AND RECOMMENDATION

Overall, the analytical results demonstrate that the coexistence equilibrium acts as a global attractor for the system. All state variables remain bounded and converge to stable long-term values regardless of their initial conditions. The results reveal that nutrient recycling, phytoplankton productivity, zooplankton grazing, oxygen regeneration, and greenhouse gas removal collectively generate strong stabilizing feedback mechanisms that enhance ecosystem resilience.

From the perspective of ocean deoxygenation, the findings suggest that healthy plankton-mediated oxygen production can offset substantial oxygen losses arising from warming, respiration, and decomposition. Thus, preserving plankton ecosystem integrity may play a critical role in mitigating the long-term impacts of climate-induced ocean deoxygenation and maintaining the sustainability of marine ecosystems.

ISSN No. 2321-2705 | DOI: 10.51244/IJRSI |Volume XIII Issue VI June 2026

Future work should include a rigorous delay-induced bifurcation analysis to establish the critical delay values at which the proposed model undergoes qualitative transitions in its dynamical behaviour.

REFERENCES

1. Achimugwu, P. U., Kinyanjui, M. N., & Malonza, D. M. (2023). Mitigation of climate change due to excessive carbon dioxide emission and accumulation: a mathematical model approach. Commun. Math. Biol. Neurosci., 2023, 70.
2. Akagha, S. C., Nwankwo, D. I., & Yin, K. (2020). Dynamics of nutrient and phytoplankton in Epe Lagoon, Nigeria: possible causes and consequences of reoccurring cyanobacterial blooms. Applied Water Science, 10(5), 109.
3. Carpenter, S. R., Caraco, N. F., Correll, D. L., Howarth, R. W., Sharpley, A. N., &Smith, V. H. (1998). Nonpoint pollution of surface waters with phosphorus and nitrogen. Ecological Applications, 8(3), 559–568.
4. Cheng, L., Abraham, J., Trenberth, K. E., Boyer, T., Mann, M. E., & Zhu, J. (2024). New record ocean temperatures and related climate indicators in 2023. Advances in Atmospheric Sciences, 41(6), 1068–1082.
5. Chowdhury, P. R., Banerjee, M., & Petrovskii, S. (2024). A two-timescale model of plankton–oxygen dynamics predicts formation of oxygen minimum zones and global anoxia. Journal of Mathematical Biology, 89(1), 8.
6. Devlin, M., & Brodie, J. (2023). Nutrients and eutrophication. In Marine pollution– monitoring, management and mitigation (pp. 75–100). Springer.
7. Gruber, N., Clement, D., Carter, B. R., Feely, R. A., Van Heuven, S., & Hoppema, M. (2019). The oceanic sink for anthropogenic CO2 from 1994 to 2007. Science, 363(6432), 1193–1199.
8. Laffoley, D., & Baxter, J. M. (2019). Ocean deoxygenation: Everyone's problem-causes, impacts, consequences and solutions. IUCN Gland, Switzerland.
9. Macdonald, J. C., & Gulbudak, H. (2023). Forward hysteresis and hopf bifurcation in an npzd model with application to harmful algal blooms. arXiv preprint arXiv:2307.06234.
10. Misra, A. K., Singh, R. K., Tiwari, P. K., Khajanchi, S., & Kang, Y. (2020). Dynamics of algae blooming: effects of budget allocation and time delay. Nonlinear Dynamics, 100(2), 1779–1807.
11. Mukherjee, N., Ghorai, S., & Banerjee, M. (2019). Detection of turing patterns in a three species food chain model via amplitude equation. Communications in Nonlinear Science and Numerical Simulation, 69, 219–236.
12. NOAA. (2024, June 16). Ocean oxygen. https://oceanservice.noaa.gov/facts/ ocean-oxygen.html. (National Oceanic and Atmospheric Administration)
13. Ochieng, F. O. (2024). A novel data-driven dynamical model for predicting future climate trends. Modeling Earth Systems and Environment, 10(4), 4599–4610.
14. Octavina, C., Maghfirah, M., Lacroix, G., Suciati, N., Fajar, M., Syufi, N. H., & Haditiar, Y. (2025). Spatial analysis of plankton distribution in northern waters of aceh: An indicator of marine environmental quality. In Bio web of conferences (Vol. 156, p. 02005).
15. Pachiappan, P., Santhanam, P., Begum, A., & Balaji Prasath, B. (2019). An introduction to plankton. Basic and applied phytoplankton biology, 1–24.
16. Prentice, I. C., Farquhar, G., Fasham, M., Goulden, M. L., Heimann, M., & Jaramillo, V. (2001). The carbon cycle and atmospheric carbon dioxide. Climate change 2001: the scientific basis, Intergovernmental panel on climate change.
17. Rehim, M., Zhang, Z., & Muhammadhaji, A. (2016). Mathematical analysis of a nutrient– plankton system with delay. SpringerPlus, 5, 1–22.
18. Rhein, M., Rintoul, S. R., Aoki, S., Campos, E., Chambers, D., Feely, R. A. & (2013). Observations: ocean.
19. Roy, S., Broomhead, D. S., Platt, T., Sathyendranath, S., & Ciavatta, S. (2012). Sequential variations of phytoplankton growth and mortality in an npz model: A remote-sensingbased assessment. Journal of Marine Systems, 92(1), 16–29.
20. Schmidtko, S., Stramma, L., & Visbeck, M. (2017). Decline in global oceanic oxygen content during the past five decades. Nature, 542(7641), 335–339.

ISSN No. 2321-2705 | DOI: 10.51244/IJRSI |Volume XIII Issue VI June 2026

21. Sekerci, Y., & Ozarslan, R. (2020). Respiration effect on plankton–oxygen dynamics in view of non-singular time fractional derivatives. Physica A: Statistical Mechanics and its Applications, 553, 123942.
22. Sterpu, M., Rocs, oreanu, C., Efrem, R., & Campbell, S. A. (2023). Stability and bifurcations in a nutrient–phytoplankton–zooplankton model with delayed nutrient recycling with gamma distribution. Mathematics, 11(13), 2911.
23. Solomon U A, Adamu I. I., Benshak S. M(2026). Mathematical Model for The Dynamics of Nutrient-Phytoplankton System with Delay Under Climate Change and Deoxygination of Oceans. Iconic Research And Engineering Journals,10(1).doi: https://doi.org/10.64388/IREV10I1-1719581.
24. Yang, H (2022). Global dynamics of a diffusive phytoplankton-zooplankton model with toxic substances effect and delay. Mathematical Biosciences and Engineering, 19(7), 6712–6730.
25. Zhuang, K, Jia, G, &Liu, D (2019). Stability and hopf bifurcation in a three-component planktonic model with spatial diffusion and time delay. Complexity, 2019(1), 4590915.